

No QPO time lags from Sco X-1 as seen with EXOSAT: a comparison with Cyg X-2.

Stefan W. Dieters^{1,2*}, Brian A. Vaughan^{1,3}, Erik Kuulkers^{1**}, Frederick K. Lamb⁴, and Michiel van der Klis¹

¹ Astronomical Institute “Anton Pannekoek”, University of Amsterdam and Center for High Energy Astrophysics, Kruislaan 403, 1098 SJ Amsterdam, The Netherlands.

² Max-Planck-Institut für Astrophysik, Postfach 15 23, D-85740 Garching b München, Germany.

³ Div. of Physics, Mathematics, and Astronomy, Caltech, Pasadena, CA 91125, U.S.A.

⁴ Departments of Physics and Astronomy, University of Illinois at Urbana-Champaign, 1110 W. Green Street, Urbana, IL 61801, U.S.A.

November 11, 2018

Abstract. We have measured the phase-delay and rms amplitude spectra of Cyg X-2 and Sco X-1. Using EXOSAT data from the normal branch of Cyg X-2 we confirm earlier (Ginga) results, showing that at an energy near 6 keV there is both a minimum in the QPO rms amplitude spectrum and a 150° phase jump in the quasi-periodic oscillations (QPO) phase-delay spectrum.

Surprisingly, using EXOSAT and Ginga data, we find no evidence for a phase jump of this kind in the phase-delay spectrum of Sco X-1 on either the normal or flaring branch. Upper limits (90% confidence) of 42° can be set on any phase jump in the energy range 2–10 keV on the normal branch, and 88° on the flaring branch. The QPO rms amplitude spectrum of Sco X-1 increases steeply with energy on both the normal and flaring branches. These results suggest that the X-ray spectrum pivots about an energy of $\lesssim 2$ keV or $\gtrsim 10$ keV or that normal branch QPO of Sco X-1 does not have a pivoting spectrum. We discuss the implications of these results in terms of the radiation-hydrodynamic model for normal branch QPO.

Key words: methods:data analysis – binaries:close – stars:individual:Sco X-1, Cyg X-2 – stars:neutron – Xrays:stars

Send offprint requests to: Stefan Dieters

* Present address: SD50 NASA Marshall Space Flight Center, Huntsville, Alabama, AL 35812, U.S.A., e-mail: stefan.dieters@msfc.nasa.gov

** Present Address: Space Research Organization Netherlands, Sorbonnelaan 2, 3584 CA Utrecht, & Astronomical Institute, Utrecht University, P.O. Box 80000, 3507 TA Utrecht, The Netherlands

1. Introduction.

After the discovery of quasi-periodic oscillations (QPO) in power density spectra of the X-ray variability of GX 5–1 (van der Klis et al. 1985), QPO were also discovered in Sco X-1 (Middleditch & Priedhorsky 1986) and Cyg X-2 (Hasinger et al. 1986). Further study showed that six of the persistently bright low-mass X-ray binaries (LMXB) form a distinct group: the Z-sources (Hasinger & van der Klis, 1989). Also see the review by van der Klis, 1995).

As the energy spectrum varies in time, a Z source traces out a characteristic, Z-shaped track in a X-ray colour-colour diagram (CD) whose x-axis is the ratio of the count rates in two low-energy bands while the y-axis is the ratio of the count rates in two high-energy bands. The three branches of the Z, from top to bottom, are called the horizontal branch (HB), normal branch (NB), and flaring branch (FB).

The fast timing behaviour (millisecond to tens of seconds) is well correlated to the position of the source along its track, thus defining the state of the source. Two¹ distinct types of low frequency QPO have been identified. The horizontal branch oscillations (HBO) with frequencies between 15 and 55 Hz have been observed in Cyg X-2, GX 5–1, GX 340+0, GX 17+2, and Sco X-1. The ~ 6 Hz normal branch oscillations (NBO) are observed from all Z sources. As Sco X-1 moves from the NB to the FB the QPO frequency increases rapidly but smoothly (Priedhorsky et al. 1986, Dieters & van der Klis 1999). Apparently similar changes in frequency are seen for GX 17+2 (Penninx et al. 1990). This smooth transition in QPO fre-

¹ We do not discuss the recently discovered kilohertz QPO, from Z and Atoll sources or the 45 Hz QPO (probably HBO) in Sco X-1 found with RXTE (see review by van der Klis 1997) because they are undetectable with EXOSAT or Ginga data

quency suggests that the NBO and the flaring branch oscillations (FBO) are related phenomena. On the FB, the QPO frequency is well correlated with X-ray count rate and position along the Z-track. Other Z sources such as GX 5–1 and Cyg X-2 have relatively inconspicuous flaring branches with, so far, no FBO².

Even though the QPO cannot be directly observed with EXOSAT or Ginga, it is possible to measure the QPO properties as a function of energy using Fourier techniques applied to large amounts of high time resolution multi-channel data. We call the fractional rms variability amplitude as a function of energy the “rms amplitude spectrum”. By using Fourier cross-spectra we can measure the phase or, equivalently, the time delay between the QPO at different energies. We call the phase difference or time delay between signals as a function of photon energy the “phase-delay spectrum” and “time-delay spectrum”, respectively.

Cross spectral techniques were first applied to the HBO of Cyg X-2 by van der Klis et al. (1987). They found that the HBO at higher energies was delayed (lagged) with respect to the HBO at lower energies by several milliseconds. More recently, Vaughan et al. (1994a) have found that the phase lag increases smoothly with increasing energy for the HBO of GX 5–1.

Ginga data from Cyg X-2 when it was on its NB (Mitsuda & Dotani 1989) showed that the NBO in the high energy bands (7–18 keV) had time-lags relative to the low-energy bands (1–7 keV) of up to ~ 80 ms or equivalently 150° phase lag. This phase-lag jump occurred near 6 keV, where there is also a minimum in the rms amplitude spectrum.

Vaughan et al. (1994a) introduced a new, more sensitive, method for measuring the phase-delay spectrum. Using this method it was found that there is a sharp phase jump of $\sim 150^\circ$ at ~ 3.5 keV in the NBO of GX 5–1 (Vaughan et al. 1999). However, there was only marginal evidence for a minimum in the rms amplitude spectrum at this energy.

The combination of a $\sim 180^\circ$ phase shift and a minimum in the rms amplitude spectrum of the NBO at the same photon energy can be explained by a radiation-hydrodynamic model (Lamb 1989, Fortner et al. 1989, Miller & Lamb 1992). At near Eddington accretion rates an approximately spherical flow forms. Within this flow a global radiation-hydrodynamic mode can be excited with a frequency inversely proportional to the inflow time. Because of the high luminosities, radiation forces become important and the infall time-scale is lengthened. Consider a density enhancement at the outer boundary; as it reaches the inner boundary its interaction with the outgoing radiation increases resulting in an increase or decrease in the

radiation flux reaching the outer boundary and hence induces, via the change in radiation force, a density change in the infalling material. Whether the flux increases or decreases depends upon the relative importance of the induced luminosity or Compton scattering opacity changes. If the influence of the changes in the Compton scattering optical depth within the radial flow dominates the influence of the changes in the luminosity during the NBO and the Compton temperature of the X-ray spectrum is low enough, then the X-ray spectrum “pivots” during the oscillations (Lamb 1989, Miller & Lamb 1992). As a result, the oscillations above the pivot energy are ~ 180 degrees out of phase with the oscillations below the pivot energy and the oscillation amplitude is small near the pivot energy. The pivot energy is most sensitive to the electron temperature in the radial flow. If instead the effect of the change in the luminosity during the NBO dominates, the X-ray spectrum may oscillate but not “pivot” (Psaltis & Lamb 1999). The luminosity at the NB-FB junction, where the N/FBO frequency changes abruptly (Dieters & van der Klis 1999), is identified with the Eddington critical luminosity (Hasinger 1987). The change in QPO as Sco X-1 moves into and along the FB may be explained either by the shrinking of the radial flow region (Lamb, 1989) or the excitation of non-radial modes (Miller & Park 1995).

We applied the Vaughan et al. (1994a) method to EXOSAT data from the NB of Cyg X-2 and on the NB and FB of Sco X-1. Ginga data from the FB of Sco X-1 were also analyzed. Because instrumental dead-time can mimic a 180° phase lag between low- and high-energy fluxes, it is important to treat it carefully. The dead-time was treated differently for the EXOSAT than for the Ginga data. For Ginga data the dead-time was corrected in the time domain (Vaughan et al. 1999) whereas for the EXOSAT data the dead-time effects were corrected in the frequency domain (van der Klis et al. 1987).

Here we report, for the first time, the detection of near 180° phase lags in the NBO of Cyg X-2 with EXOSAT data. This is a direct confirmation of the results of Mitsuda & Dotani (1989), who used Ginga data. We set approximate limits on the change in pivot energy with position on the NB. No Sco X-1 data have previously been analyzed for phase lags. We find for both the NB and FB of Sco X-1 that the rms amplitude spectrum increases steeply with photon energy, with no indication of a minimum. We detect only small phase lags with no indications of any $\sim 180^\circ$ phase lags on either the NB or FB.

2. Observations

We used data from the ME detectors on-board EXOSAT (Turner et al. 1981, White & Peacock 1988) and from the LAC detectors on the Ginga satellite (Makino et al. 1987, Turner et al. 1989). The EXOSAT HER7 observing mode provided 4 energy channels of data with 4 or 8 ms time res-

² The QPO on the FB of Cyg X-2 (Kuulkers & van der Klis 1995) are thought to be of a different character than the NBO/FBO of Sco X-1 and GX 17+2

olution. Sco X-1 was observed using the HER7 mode on the NB and FB on Aug 25 (day 237) 1985 (Priedhorsky et al. 1986) and on the NB on March 13 (day 072) 1986 (Hasinger et al. 1989). The energy bands were 0.9–3.1, 3.1–4.9, 4.9–6.6, and 6.6–19.5 keV. These Sco X-1 observations were non-standard in that one half-array of 4 detectors was off-set pointed ($\sim 12\%$ collimator response), gathering HER7 data from only the argon (1–20 keV) detectors of the ME instrument, while the other half-array was pointed directly at Sco X-1 gathering high-time-resolution (HTR3 mode), single-channel (4 or 8 ms, 5–35 keV) data from only the xenon detectors of the ME instrument.

During each NB observation of Sco X-1 the QPO frequency was generally stable. Any short frequency excursions (>1 Hz away from the average) were excluded from the data to keep the average QPO peak narrow. A total of 3040 s and 5504 s of data were selected from data taken during the Aug 1985 and March 1986 observations. Both observations spanned the lower normal branch; $1.6 \leq S_Z \leq 1.9^3$. The QPO frequency was 6.41 ± 0.05 Hz (full width half maximum, FWHM, of 1.91 ± 0.14 Hz) during the Aug 1985 observation and 6.15 ± 0.05 Hz (FWHM of 2.4 ± 0.4 Hz) during the Mar 1986 observation. The EXOSAT Aug 25, 1985 observation also contained data while Sco X-1 was on the flaring branch. These data were grouped according to QPO frequency. Only in the frequency range 14.5–15.5 Hz were there sufficient data for phase-lag studies; i.e., a total of 5632 s spanning $2.06 \leq S_Z \leq 2.17$.

The Ginga data on Sco X-1 studied here were obtained using MPC-3 mode data, which consists of 12 spectral channels over the energy range 1.5–18.7 keV (high detector gain) with 8 ms time resolution. During these observations on March 9/11 1989, Sco X-1 was on the FB (Hertz et al. 1992). Data (3320 s) were selected from the lowest segment of the flaring branch where the QPO frequency was $14.5 \text{ Hz} \pm 0.3 \text{ Hz}$ (FWHM of 6.3 ± 1.3 Hz). This QPO frequency is found at Z track positions corresponding to $2.06 \leq S_Z \leq 2.09$. There are no high-time-resolution Ginga data available when Sco X-1 showed NBO.

The EXOSAT observations of Cyg X-2 were obtained on November 14/15 (day 318/319) of 1985 using the HER7 mode with a time resolution of 4 ms. During this observation which lasted ~ 13 hr, Cyg X-2 was on the NB and FB (Hasinger & van der Klis 1989, Kuulkers et al. 1996). Four energy bands (from the argon layer detectors) were available: 0.9–3.1, 3.1–4.7, 4.7–6.3, and 6.3–19.7 keV (i.e., roughly the same energy bands as used for Sco X-1). The NBO are clearly present over the range $S_Z = 1.3$ –1.7. We divided the NB into two parts: in

the ranges $1.1 \leq S_Z \leq 1.6$ (“upper NB”) and $1.6 \leq S_Z \leq 2.0$ (“lower NB”). This yielded 14048 s and 15168 s of observations for the upper NB and the lower NB, respectively. The mean QPO frequency was 5.6 ± 0.1 Hz with FWHM 2.2 ± 0.3 Hz on the upper NB and 5.8 ± 0.1 Hz with FWHM 1.7 ± 0.5 Hz on the lower NB.

3. Analysis

We first divided the data into 32 s long data segments and then calculated the individual complex Fourier transforms (CFTs). This was done for each energy channel. Then, the cross spectrum was calculated as the product of the CFT of one channel with the complex conjugate of the CFT of the other channel for each possible pair of energy channels. In each data set the cross spectra of all data segments were averaged together. The average cross spectrum thus consists of a sequence of individual cross vectors, one at each Fourier frequency. Further averaging was done in frequency to produce an average cross-vector over the QPO frequency range for each pair of energy channels.

Instrumental dead time induces an anti-correlation between energy channels that appears in the cross correlation function as an anomalously large negative value at zero lag, and in the cross spectrum as a purely negative real part in each cross vector that is independent of Fourier frequency, corresponding to a phase difference of 180° . Both Poisson fluctuations and luminosity signals induce such phase lags (Lewin et al. 1988). This effect is known as channel cross-talk. The channel cross-talk induced by the source signal (QPO) was found to be insignificant compared to that from the Poisson fluctuations (Vaughan et al. 1999) for typical QPO amplitudes and count-rates as measured with EXOSAT and Ginga.

As discussed by Vaughan et al. (1999), there are three possible approaches to handling the dead-time effects induced by Poisson fluctuations. First, a “signal-free” cross vector obtained from the data itself in a frequency range devoid of signals can be subtracted from the signal (QPO) cross vector. Second, by knowing the dead-time process, the modified probability distribution in each channel can be calculated and hence from it the induced covariance and induced dead-time cross vector, which can then be subtracted from the QPO cross vector. Last, the observed count rates (as affected by dead-time) can be converted to counts per live-time and then the corrected rates can be used in calculating the complex Fourier spectra and so the cross spectra are without the dead-time-induced negative, real component. These three methods are referred to as the frequency domain, statistical and time domain methods respectively. We used the time domain (last) method for the Ginga data and the frequency domain (first) method for the EXOSAT data.

The dead-time process for EXOSAT is complicated (Andrews 1984, Andrews & Stella 1985, Tennant 1987, Berger & van der Klis 1994) and not entirely understood.

³ The Z-track position is parameterized by S_Z , the arc length along a smooth Z-track drawn through the points on a colour-colour diagram, scaled such that $S_Z=1$ at the HB/NB vertex and $S_Z=2$ at the NB/FB vertex (see Dieters & van der Klis 1999).

Therefore it is not possible to estimate the effects of dead-time on the count-rate distribution with the required degree of precision. A time-domain count rate correction is not possible because at high count rates the dependence of dead-time on count-rate is not known precisely enough, and also because the count rates, especially in the high-energy channel are too low (≤ 1 per 4 ms time bin). There are too many zero count bins for an accurate conversion. We therefore adopted the procedure of subtracting the average real part of the observed cross spectrum at high frequencies (72–128 Hz) from the cross vector at each frequency of the cross spectrum. This procedure is similar to that used by van der Klis et al. (1987). The underlying assumption is that there is no intrinsic signal in the high-frequency region of the cross spectrum. At these frequencies, high-frequency noise is the only known source signal. Its amplitude, when QPO are detectable, is small at high frequencies since its cut-off frequency is between 60 – 80 Hz in the NB and near 35 Hz on the FB (Dieters & van der Klis 1999). Thus at high frequencies any time lags should be due to instrumental effects and so should be a good measure of the dead-time induced channel-talk. The imaginary part of the high-frequency vector should be ignored because the dead-time-induced vector is purely real. In all cases we found a large negative real vector, and the distribution of the imaginary part, at high frequencies, was consistent with a null-mean normal distribution (a large number of estimates were averaged, so the central limit theorem applies) with a variance due only to counting statistics.

For Ginga data the dead-time process is better understood and, moreover, count rates in all energy channels are high enough to correct them in the time domain. We used the known, fixed dead-time per event to correct the counts in each time bin and in each energy channel to counts per live time, before computing cross spectra (Mitsuda & Dotani 1989, Vaughan et al. 1999).

After calculating the cross spectra and applying the above dead-time correction strategies, the average signal cross vectors were calculated for each energy channel pair by averaging over the frequency range of the QPO peak. The signal frequency range used was $\nu_c \pm (3/4)\Delta\nu$ Hz, where ν_c is the QPO centroid frequency and $\Delta\nu$ is its FWHM. For the EXOSAT data, the error estimates in the average signal cross vectors are based upon the observed variance in the individual values of the real and imaginary components of both the high-frequency vector and the QPO vector. These error estimates are consistent with the error expected from counting statistics, given the count rates, rms amplitude of the QPO, and length of the observations and assuming perfect coherence between channels for the QPO. For the Ginga data the errors were directly estimated from the cross vectors given the number of frequencies and Fourier transforms used (equation 11 of Vaughan et al. 1994a).

Because QPO are weak compared with counting (Poisson) noise, measuring phase differences involves first setting a detection threshold on the magnitude of the average “signal” cross vector and then, only in the case of significant detection, setting confidence limits on the phase. Conceptually and computationally, the procedure is similar to detecting and measuring coherent pulsations (Vaughan et al. 1994b).

Each of the terms averaged together in estimating the average cross vector of the QPO is the product of two complex random variables whose real and imaginary parts each have a Gaussian distribution with a null mean. In the absence of a source signal, the real and imaginary parts of the average cross vector are themselves distributed as null-mean Gaussian random variables and the squared magnitude of the average cross spectrum, $|G|^2$, is distributed as $\exp(-|G|^2/|G_0|^2)$, where $|G_0|^2$ can be well estimated from the variances in the real and imaginary parts of the cross spectrum. The phase angle (argument) of G is distributed uniformly over $[-\pi, +\pi]$.

A significant detection is when the magnitude of the signal cross vector is greater than some previously chosen detection threshold. We chose a 95% confidence detection threshold for all cross spectra. If the average cross vector fails to exceed the detection threshold, we can conclude nothing about the presence or absence of phase differences (angle of cross vector) or place any meaningful limits on their size. Either the QPO signal is too weak compared with the noise background to allow a significant detection, or the signals in the different channels were not sufficiently coherent (Vaughan et al. 1994a).

Once a significant detection of the cross vector is made, the phase delay (the argument or phase angle of the signal cross vector) can be found. We determined the 90% confidence intervals of the phase angle. Naturally the phase delay can be zero when the cross vector is significant. In this case we can set a meaningful upper limit on the phase delay.

For both the EXOSAT and Ginga data we used the χ^2 method of Vaughan et al. (1994a), which makes use of all available information by taking into account all statistically significant cross-vectors between each possible combination of channels. Similar but less significant results were obtained by only using the cross vectors between the lowest energy channel and each of the other channels.

Towards the lowest and highest energies measured by EXOSAT and Ginga the PHA spectrum of both sources drops steeply. At low energies this is because of interstellar absorption while at high energies it is due to a combination of the steep intrinsic energy spectrum and a drop in detector efficiency. Thus the central energies, particularly of the lowest and highest, and necessarily broadest channels, used to measure the rms amplitude and phase do not reflect the energy of most of the photons being measured. We can define the photon-average central energy as the energy which splits the number of photons evenly within

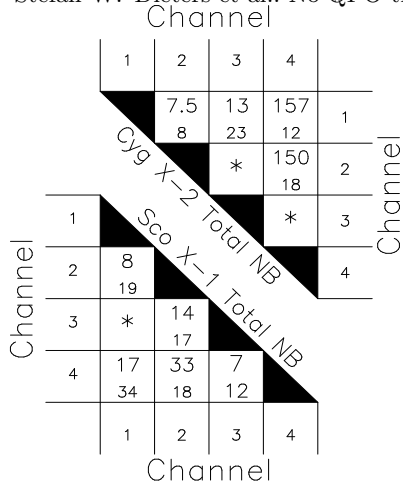


Fig. 1. The channel by channel results for the cross-spectral analysis of the EXOSAT data for Cyg X-2 and Sco X-1. The upper panel is for the NBO of Cyg X-2 from data covering both the upper and lower sections of the NB. The lower panel is for the NBO of Sco X-1 using the sum of the NB data from 25 Aug 1985 and 13 March 1986. In each box the upper number is the measured phase lag in degrees while the lower number is the 90% uncertainty. A * indicates that the magnitude of the average cross vector is *not* significant.

the channel’s range. The photon average central energy of the lowest and highest HER7 channels were measured with multi-channel (32 or 128 channel) ME Ar data taken on on Aug 3 (day 216) 1984 and Jun 26/27 (day 177/178) 1985, respectively. All 12 channels of the Ginga MPC-3 data were used to find these limits for Sco X-1 on the FB. These half-count-rate energies are 2.3 and 9.6 keV, 2.9 and 12.0 keV for the EXOSAT and Ginga data for Sco X-1 respectively, and 2.4 and 7.0 keV for the EXOSAT Cyg X-2 data.

Although, to first order, the theoretical rms amplitude spectrum (Miller and Lamb 1992) can be directly compared with our observed rms spectrum, to do a comparison good enough to place limits on pivot energy requires folding a fine grid of models through the detector matrix. Modeling the observed phase lag spectrum would require, in addition to knowing the PHA spectrum, assumptions about the variation of rms amplitude and phase with energy within each energy channel. Given the current state of our knowledge we only provide general statements about the energy of any phase jump.

4. Results

4.1. Cyg X-2.

For Cyg X-2 (EXOSAT data) we determined time/phase delays in three independent frequency intervals, one centered on and covering the NBO ($\nu_{NBO} \pm \frac{3}{4} \Delta\nu$, i.e. 4.2–7.2 Hz) and two (1.2–4.2 and 7.2–10.2 Hz) on each side of the NBO peak in the power spectrum. In the frequency

ranges adjacent to the NBO we found no significant cross vectors between any pair of energy channels.

In the NBO frequency range, particularly on the upper normal branch, we found several significant cross vectors which showed a large phase/time delay between the two highest channels (3 and 4) and no significant delays between the lower energy channels (Fig. 2). The actual channel by channel detections, for the whole NB, are given in the upper part of Fig 1.

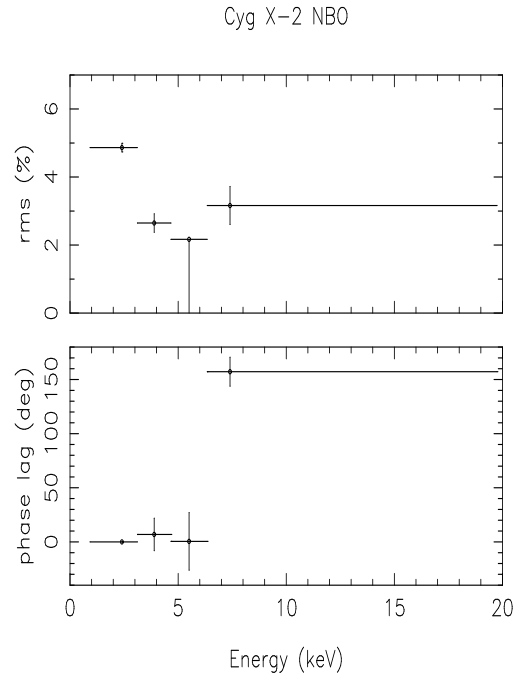


Fig. 2. The rms amplitude spectrum and phase delay spectrum from EXOSAT data for the NBO of Cyg X-2, averaged over the part of the NB where the NBO is detectable. A 2σ upper limit is shown for the rms amplitude in channel 3. The 1σ limit is 0.5% rms. The phase delays are with respect to channel 1, so this channel has no error bar.

We determined a mean rms amplitude (energy) spectrum of the NBO. We fixed the NBO centroid frequency at 5.7 Hz and the FWHM at 2.0 Hz, the values obtained from a fit to the power spectra of the sum of channels 1–4, and allowed only the strength of the NBO to vary in our fits to the power spectra of the individual channels. There is a dip at channel 3 (4.7–6.3 keV) in the rms amplitude spectrum (2σ upper limit in Fig. 2).

We find that the rms amplitude spectra and the phase delay spectra are the same within the 1σ errors on the upper and lower branch. Since the dips in the model rms amplitude spectra are comparable in width (~ 1.8 keV) to the width of channel 3, a change in pivot energy to an adjacent energy bin; i.e. to the middle of channel 2 (3.9 keV) or to the photon average central energy of channel 4 (7 keV) would cause a large change in the rms amplitude spec-

trum. So we conclude that the pivot energy did not change more than $\sim\pm 1.5$ keV along the NB. As a comparison with the models (Miller & Lamb 1992); a change in electron temperature from 0.5 to 1.0 keV changes the pivot energy from 5.2 to 7.3 keV and so can be excluded.

In the upper NB the higher energy time/phase delay amounted to 78 ± 4 ms or equivalently $161\pm 9^\circ$. In the lower NB the time/phase lags were very similar, i.e.; 70 ± 6 ms or alternatively $144\pm 12^\circ$. Averaged over the whole NB the time/phase delays were 75 ± 4 ms or $154\pm 7^\circ$. Considering the source energy spectrum and model rms amplitude spectra, the pivot energy should reasonably lie between (approximately) the middle of channel 3 (5.5 keV) and photon average central energy of channel 4 (7 keV). We therefore conclude that the pivot energy is near 6 keV.

Our results confirm, using another instrument (the EXOSAT ME), the existence of both a near- 180° phase jump and a rms amplitude minimum in Cyg X-2 as previously seen by Mitsuda & Dotani (1989) using Ginga LAC data. Because the instrumental dead-time effect produces a 180° phase delay, it is reassuring that the results found with two different instruments are in complete agreement.

4.2. Sco X-1.

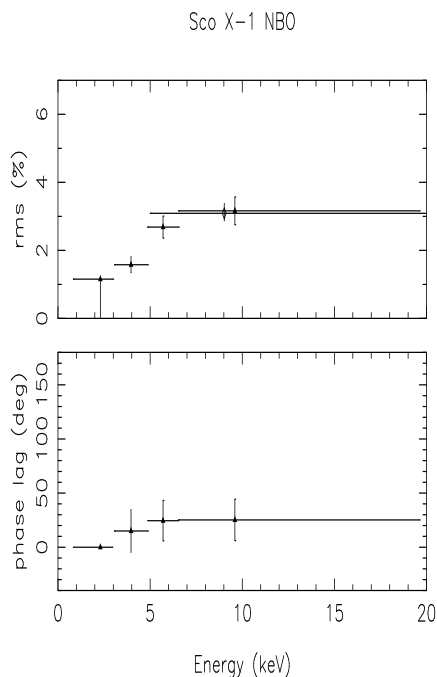


Fig. 3. The rms amplitude spectrum and phase delay spectrum from EXOSAT data on the NBO of Sco X-1, averaged over the Aug 25, 1985 and March 13, 1986 data sets. The phase delays are with respect to channel 1 on so this channel has no error bar.

For the NB EXOSAT data from Sco X-1, we determined the phase/time lags over the frequency range spanning the NBO peak ($\nu_{NBO} \pm \frac{3}{4} \Delta\nu$) and also over several other frequency ranges for each data set (Aug 25 1985 and March 13 1986) separately. We found no significant cross-vectors for any of the non-QPO frequency ranges. The data, particularly from 13 March 1986 (day 072), were of sufficient quality to detect significant QPO cross vectors. Our channel-by-channel detections for the sum of the NB data are listed in the lower part of Fig. 1. At the 90% confidence level we found no phase delays in the NB greater than 60° (largest limit in both data sets) between any pair of energy channels. By combining both data sets, an overall upper limit of 42° (highest possible phase lag using the χ^2 method) at the 90% confidence level can be set on any phase jump on the NB between ~ 2.3 and 9.6 keV (photon average central energies of channels 1 and 4 respectively). The phase delay spectrum is shown in the lower panel of Fig. 3. The separate rms amplitude spectra and also the average of both observations (upper panel of Fig. 3) show no sign of a dip.

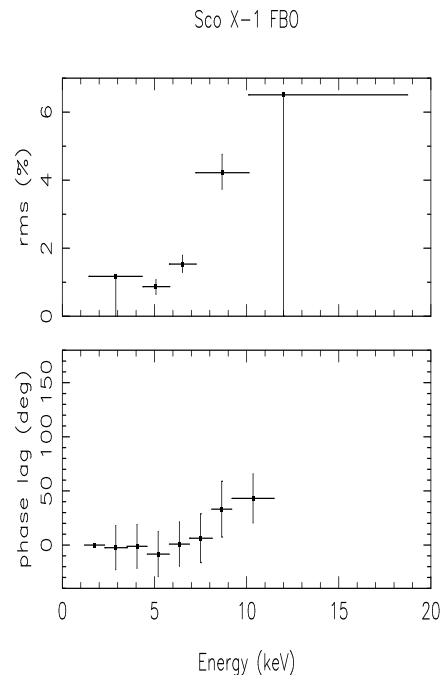


Fig. 4. The rms amplitude spectrum and phase delay spectrum from Ginga data for the FBO of Sco X-1. The phase delays are with respect to channel 1 on so this channel has no error bar. When a phase delay is not significant it has been omitted from the plot. Some correlation in phase lag between adjacent bins is introduced by the χ^2 method.

The EXOSAT FB data were of sufficient quality only to measure the phase delay between channels 2 and 3. In the 10–20 Hz range covering the QPO, this delay was

consistent with zero (90% confidence upper limit of 22°). No significant cross-vectors were found for other frequency ranges. These tests included frequencies typical of NBO.

The Ginga FB data showed significant cross vectors between all channels, except those at the lowest and highest energies (lower panel of Fig. 4) where the QPO signal is very weak, as can be seen in the rms energy spectrum of the upper panel of Fig. 4. Again, the phase delays were consistent with zero. The 90% confidence upper limit on any phase lag between channels 1 to 8 (energy range 2.9–12 keV) is 88° (between 4.5 and 8.1 keV this value is 51.4°). The rms energy spectrum on the FB has a similar form to that on the NB, with no evidence for a dip.

5. Discussion

Our methods are capable of detecting a phase jump in EXOSAT data as is evidenced by our clear detection of such a jump for Cyg X-2, confirming the result of Mitsuda & Dotani (1989). For Sco X-1 we find no evidence for a phase jump or minimum in the rms amplitude spectrum in the range 2–10 keV on the NB, or 3–12 keV on the FB, with 90% confidence upper limits on the size of such a phase jump of 42 and 88 degrees, respectively. Either Sco X-1 does not have a rocking NBO spectrum or the pivot energy is either $\lesssim 2$ keV or $\gtrsim 10$ keV. In view of the fact that the rms amplitude is steeply increasing with energy much like the expected rms spectrum above the pivot energy (Miller & Lamb 1992), we favour the lower possible pivot energy. This is clearly different from the pivot energy of Cyg X-2 which is close to 6 keV (Mitsuda & Dotani 1989, this paper) and GX 5–1 at about 3.5 keV (Vaughan et al. 1999).

In many respects all the Z sources are very similar. In particular the behaviour of the NBO is nearly identical between sources. An exception may be GX 349+2 (Kuulkers & van der Klis, 1998). So it is initially a surprise that the pivot energy should be so different (factor 2-3). This is particularly the case for Cyg X-2 and GX 5–1 which based upon source behaviour are considered more alike than either compared to Sco X-1.

Nearly all behavioural properties of the Z sources are solely a function of Z track position. Several arguments identify the mass accretion rate as governing the Z track position. Also the nature of the accretion flow is apparently dependent on \dot{M} relative to the Eddington accretion rate \dot{M}_{Edd} . A comparison between Z sources (Dieters & van der Klis 1999) has shown that the NBO become detectable at much the same Z track position suggesting that S_Z is an accurate measure of \dot{M} relative to \dot{M}_{Edd} across Z sources.

We considered as did Vaughan et al. (1999) whether the different pivot energies in different sources are due to sampling a pivot-energy/ \dot{M} relation at different mass accretion rates. This seems unlikely because the estimated \dot{M} 's are comparable for all Z sources in the same spec-

tral branch (Hasinger & van der Klis 1989, Hasinger et al. 1990, Vrtilik et al. 1990). More sensitively, \dot{M}/\dot{M}_{Edd} must be very similar to produce NBO (Lamb 1989, Fortner et al. 1989, Miller & Lamb 1992). Confirming that changes in \dot{M} on the NB make little difference is our observation that the pivot energy does not change greatly (± 1.5 keV) along the NB of Cyg X-2. Our NB observations of Sco X-1 were made at very similar Z track positions as the lower NB observation for Cyg X-2. Also, for Sco X-1 the phase-lag and rms-energy spectra are similar on the NB and FB despite the radically different flow conditions associated with sub (NB) and super (FB) critical Eddington accretion.

Based upon differences in the HB and FB morphologies and the relative strengths of the FBO there seem to be two groups, of Z sources: those like Cyg X-2 and those like Sco X-1. These two sources may represent the extremes in a continuum of properties. The Sco-like sources are Sco X-1, GX 17+2, and GX 349+2 and the Cyg-like sources are Cyg X-2, GX 5–1, and GX 340+0. Both inclination angle (Hasinger & van der Klis 1989, Kuulkers et al. 1994, 1996) and neutron star magnetic field strength (Psaltis et al. 1995, Psaltis & Lamb 1999) have been put forward as the underlying factor giving rise to these two groups.

The fact that phase jumps are observed in GX 5–1 and Cyg X-2 and not in Sco X-1 is consistent with this division into two groups. If this subdivision can indeed be applied to phase delays in Z sources, then in the energy range above ~ 2 keV we expect to see a phase jump in the NBO of GX 340+0, whereas no such phase jump is expected for GX 17+2 and GX 349+2.

The rms amplitude spectrum of GX 17+2 shows no dip between ~ 5 keV and ~ 12 keV on either the normal or flaring branches (Penninx et al. 1990). Similarly there is no evidence for a dip in the NBO rms amplitude spectrum of GX 349+2 above ~ 5 keV, and there is no phase lag/lead between low (1–5 keV) and high (5–10 keV) photons $\geq 80^\circ/118^\circ$ (90% confidence) (Ponman et al. 1988). These measurements are consistent with both sources being Sco-like. In the case of GX 340+0, a Cyg-like source the rms amplitude spectrum shows no dip at $\gtrsim 5$ keV. A dip such as that of Cyg X-2 is probably excluded but this source may be like GX 5–1 with a low pivot energy. The above evidence is broadly consistent with the pivot energy also being related to the division of Z-sources into two groups.

If, pivot energy depends upon inclination angle, say through asymmetries in the QPO production region caused by the presence of an inner ‘‘puffed-up’’ torus, then this could explain the differences between Cyg X-2 and Sco X-1. However, the pivot energies of Cyg X-2 and GX 5–1 are reversed with the assumed ranking of sources by inclination angle within the Cyg X-2 group as proposed by Kuulkers & van der Klis (1995).

In the radiation-hydrodynamic model (Lamb 1989, Fortner et al. 1989, Miller & Lamb 1992), the N/FBO are

produced in a relatively cool, spherically symmetric, radial inflow region that surrounds a hotter inner corona and magnetosphere of the neutron star. The assumption of approximately spherical symmetry eliminates inclination as causing the differentiation of the Z-sources. Recent extensions to the basic model have suggested that the neutron star magnetic field strength is the controlling factor (Psaltis et al. 1995, Psaltis & Lamb 1999).

If the NB/FBO is caused by a radiation force - opacity feedback mechanism, where the opacity is primarily due to Compton scattering, then the small changes in optical depth during each oscillation will cause the energy spectrum to pivot (Lamb 1989). As a natural consequence, there is a minimum in the rms amplitude spectrum of the QPO and about a 180° phase jump at the pivot energy in the phase lag spectrum. This appears to be the case for Cyg X-2. The longer escape time of photons scattered downward in energy by the cool radial flow may explain why the observed phase shift is not exactly 180 degrees (Lamb 1989).

The pivot energy depends mainly, though weakly, upon the electron temperature (T_e) of the cool radial flow and to a lesser extent on its optical depth τ . The electron temperature can be estimated fairly accurately by computing the Compton temperature of the X-ray spectrum we observe. The possible values for the optical depth are limited by the twin constraints of the observed spectrum and the lack of any X-ray pulsations. In the simplified spectral model of Miller & Lamb (1992) the value of T_e needed to fit the data of Mitsuda & Dotani (1989) and presented here for the Cyg X-2 NBO is the same as the value of T_e computed from the observed spectrum of Cyg X-2. Given the range of Compton temperatures determined from the X-ray spectra of Z-sources (0.5–1.5 keV), the range of possible pivot energies is limited to those shown in Figure 5 of Miller & Lamb (1992), i.e. 5–10 keV. This is incompatible with the observed energy of the phase jump (~ 3.5 keV) of GX 5–1 and the implied pivot energy (≤ 2.3 or ≥ 9.6 keV) for Sco X-1.

If, instead of optical depth modulations dominating during NBO, the effect of the luminosity changes dominates, then the X-ray spectrum may oscillate without pivoting (Psaltis & Lamb 1999). Modeling of the shapes of the Z tracks of various sources (Psaltis et al. 1995) requires that the neutron stars in the Sco-like subclass of Z sources have weaker magnetic fields than the neutron stars in the Cyg-like subclass. A weaker magnetic field will produce a softer radiation spectrum from the magnetosphere and hot central corona. The shape and luminosity of this softer spectrum is affected more by changes in the mass flux than the spectrum emerging from a stronger field neutron star, so luminosity changes may dominate NBO production, accounting for the lack of any evidence for a pivoting spectrum in Sco X-1.

However, this does not explain why GX 5–1 has a phase-jump (pivot) energy lower than the range compat-

ible with the models of Miller & Lamb (1992) used successfully for Cyg X-2.

5.1. Conclusion

There are two possible sets of explanations for the results presented here for Sco X-1 and Cyg X-2 and for those on GX 5–1 (Vaughan et al. 1999). First; there may be asymmetries in the NBO producing region causing the pivot energy to depend upon viewing angle (i.e., inclination).

Second, within the context of the radiation-hydrodynamic models for the NBO/FBO, the QPO of Cyg X-2 and GX 5–1 are dominated by optical depth changes while those of Sco X-1 are dominated by luminosity variation, the underlying cause of the differences in QPO production being due to the neutron star of Sco X-1 having weaker magnetic field. Both explanations are at this stage unable to account for all details of the distribution of the measured pivot energies over the sources.

Acknowledgements. We wish to thank Guy Miller who supplied, in tabular form, the results of NBO models as presented in Miller and Lamb (1992) and Demetrios Psaltis for valuable comments. This work was supported in part by the Netherlands Organization for Scientific Research (NWO) under grant PGS 78-277. At the Max Planck Institute for Astrophysics S. Dieters was supported by grant ERB-CHRX-CT93-0329 of the European Commission (HCM program). Brian Vaughan acknowledges support from NASA under grant NAG 5–3293.

- Andrews D., 1984, EXOSAT Express 5, 31.
 Andrews D., & Stella L., 1985, EXOSAT Express 10, 35.
 Berger M., & van der Klis M., 1994, A&A 293, 175.
 Dieters S.W., & van der Klis M., 1999, MNRAS, in press, astro-ph/9909472
 Fortner B., Lamb F.K., & Miller G.S., 1989, Nat 342, 775.
 Hasinger G., 1987, A&A 186, 153.
 Hasinger G., & van der Klis M., 1989, A&A 225, 79.
 Hasinger G., Langmeier A., Sztjanjo M., et al. 1986, Nat 319, 469.
 Hasinger G., Priedhorsky W.C., & Middleditch J., 1989, ApJ 337, 843.
 Hasinger G., van der Klis M., Ebisawa K., Dotani T., & Mitsuda K., 1990, A&A 235, 131.
 Kuulkers E., & van der Klis M., 1995, A&A 303, 801.
 Kuulkers E., & van der Klis M., 1996, A&A 314, 567.
 Kuulkers E., & van der Klis M., 1998, A&A 332, 845.
 Kuulkers E., van der Klis M., Oosterbroek T., et al. 1994, A&A 289, 795.
 Kuulkers E., van der Klis M., Vaughan B.A., 1996, A&A 311, 197.
 Lamb F.K., 1989 in: Two Topics in X-ray Astronomy, 23rd ESLAB Symp., J. Hunt & B. Batrick (eds.) 1989, ESA SP-296, v1, p. 215.
 Lewin W.H.G., van Paradijs J., van der Klis M., 1988, Sp. Sci. Rev. 46, 273.
 Makino F. and ASTRO-C Team, 1987, Astr. Lett. Comm. 25, 233.

- Middleditch J., & Priedhorsky W.C., 1986, ApJ 306, 230.
- Miller G.S., & Lamb F.K., 1992, ApJ 388, 541.
- Miller G.S., & Park, M-G., 1995, ApJ 440, 771.
- Mitsuda K., & Dotani T., 1989, PASJ 41, 557.
- Penninx W., Lewin W.H.G., Mitsuda K., et al. 1990, MNRAS 243, 114.
- Priedhorsky W., Hasinger G., Lewin W.H.G., et al. 1986, ApJ 306, L91.
- Ponman T.J., Cooke B.A., & Stella L., 1988, MNRAS 231, 999.
- Psaltis D., Lamb F.K. & Miller G.S. 1995, ApJ 454, L137.
- Psaltis D., & Lamb F.K. 1999, in preparation.
- Tennant A.F., 1987, MNRAS 226, 963.
- Turner M.J.L., Smith A., & Zimmermann H.U., 1981, Sp. Sci. Rev. 30, 513.
- Turner M.J.L., Thomas H.D., Patchett B.E. et al. 1989, PASJ 41, 345.
- van der Klis M., Jansen F., van Paradijs J. et al. 1985, Nat 316 225.
- van der Klis M., 1995, In *X-ray Binaries*, W.H.G. Lewin, J. van Paradijs, & E.P.J. van den Heuvel (eds.), Cambridge Univ. Press, Great Britain, pp252-307.
- van der Klis M., Hasinger G., Stella L., et al. 1987, ApJ 319, L13.
- van der Klis M., 1997, in NATO/ASI Ser, The Many Faces of Neutron Stars, ed R. Buccheri, J. van Paradijs, & M.A. Alpar (Dordrecht: Kluwer), astro-ph/9710016
- Vaughan B.A., van der Klis M., Lewin W.H.G., et al. 1994a, ApJ 421, 738.
- Vaughan B.A., van der Klis M., Wood K.S., et al. 1994b, ApJ 435, 362.
- Vaughan B.A., van der Klis M., Lewin W.H.G., et al. 1999, A&A 343, 197.
- Vrtilek S.D., Raymond J.C., Garcia M.R., et al. 1990, A&A 235, 162.
- White N.E., & Peacock A., 1988, in: X-ray Astronomy with EXOSAT, R. Pallavicini & N.E. White (eds.), Mem. S. A. It. 59, 7.